Phase transitions in classical two-dimensional lattice Coulomb gases

Jong-Rim Lee and S. Teitel
Department of Physics and Astronomy, University of Rochester, Rochester, New York 14627
(Received 16 January 1992; revised manuscript received 13 April 1992)

We carry out Monte Carlo simulations of the two-dimensional classical neutral Coulomb gas of integer charges on a square and a triangular lattice, and find rich phase diagrams as a function of temperature and chemical potential. At high densities, the ground state becomes a periodic charge lattice, and we find evidence suggesting that the melting transitions of these charge lattices are not always in the universality class expected from symmetry analysis. We compute the inverse dielectric constant ϵ^{-1}, which vanishes at the "metal-insulator" transition of the Coulomb gas. When the ground state is a charge vacuum, we find that ϵ^{-1} is well described by the Kosterlitz-Thouless (KT) theory. When the ground state is a charge lattice, a larger than the KT universal jump in $\epsilon^{-1}(T_c)$ may be present. We also carry out simulations of the $f=\frac{1}{2}$ and $\frac{1}{3}$ fractional Coulomb gas on a triangular lattice, and find similar results.

I. INTRODUCTION

Two-dimensional models of logarithmically interacting charges,[1] referred to as the "Coulomb gas" (CG), have found wide application in understanding the behavior of many different physical systems. Via a mapping to the XY model,[2,3] the neutral "integer" Coulomb gas, consisting of equal numbers of positive and negative integer charges, serves as a model for vortex interactions in thin superconducting[4] and superfluid[5,6] ^{4}He films. In this system, in the low-charge-density limit, one finds the well-known Kosterlitz-Thouless (KT) transition.[2] At low temperatures, all charges are bound together in neutral pairs. As the temperature is increased, a critical temperature T_c occurs at which the neutral pairs unbind to give a conducting charge fluid. At T_c, the inverse dielectric function of the charges ϵ^{-1} jumps discontinuously from the finite universal value $4T_c$ to zero.[2] ϵ^{-1} of the Coulomb gas may be mapped[6,7] onto the "helicity modulus" of the corresponding XY model, where its vanishing signals the loss of phase coherence.[3] The "fractional" Coulomb gas, consisting of a finite fraction f of positive integer charges on a uniform neutralizing background charge, maps onto the class of "uniformly frustrated" XY models, which model behavior in superconducting films,[1(a)] and Josephson-junction arrays,[8,9] in a transverse applied magnetic field. Here the positive integer charges form a periodic lattice in the ground state, modeling the vortices induced by the magnetic field, as in the mixed phase of a type-II superconductor. Other physical systems, such as two-dimensional melting, surface roughening, and liquid crystals, can also be described in terms of logarithmically interacting topological defects.[10] Thus, it is desirable to have a complete understanding of behavior in the Coulomb gas.

Despite the general acceptance of the Kosterlitz-Thouless mechanism at low charge (vortex) densities, there remain many incompletely understood aspects of the Coulomb gas. Extending the KT recursion equations to higher order in the charge fugacity, Minnhagen[11] has proposed a phase diagram in which, at sufficiently high charge density, the transition from insulator to conductor becomes first order,[12] with a larger jump in ϵ^{-1} than the KT universal value. For the case of the fractional Coulomb gas, it is still poorly understood how the additional excitations of the ground-state charge lattice, which may involve large domains, interact with the pairwise excitations of the KT theory. Even in the simplest case, corresponding to the $f=\frac{1}{2}$ or fully frustrated XY model, there are conflicting estimates as to whether or not the vanishing of ϵ^{-1} occurs at the same temperature at which the charge lattice melts,[8,13,14] as well as whether the jump in ϵ^{-1} at T_c is the universal KT value.[14,15] The nature of the melting transition of the charge lattice in this model is also unclear. Most investigations[8,13,16] found evidence that this melting transition was in the Ising universality class, as would be expected from a Landau-like symmetry analysis. Recently, however, Kosterlitz and co-workers,[17] using a different finite-size-scaling method, have suggested that the critical behavior is not Ising-like and may exhibit nonuniversal features, depending, for example, on the geometry of the lattice.

In order to investigate these issues, we present here the results of extensive Monte Carlo studies of the two-dimensional Coulomb gas on both square and triangular lattices. This paper contains the details of two earlier works[18] as well as several additional results. For the integer CG, we add a chemical potential to explicitly vary the charge density, and study behavior in the dense limit. We find very rich phase diagrams, including ordering into periodic charge lattices, which melt by transitions which do not always appear to be in the universality class expected from a symmetry analysis. We also study several cases of the fractional CG on the triangular lattice and find similar behavior. The rest of this paper is organized as follows. In Sec. II, we define the two-dimensional lattice Coulomb gas model, discuss our Monte Carlo algorithm, and review the finite-size-scaling

methods we will use to determine the critical behavior of the system. In Secs. III and IV, we present our results for the integer CG on the square and triangular lattices, respectively. In Sec. V, we present results for the fractional CG on a triangular lattice, for the cases $f=\frac{1}{2}$ and $\frac{1}{3}$. In Sec. VI, we present our conclusions.

II. THE COULOMB GAS MODEL AND METHODS OF ANALYSIS

A. The lattice Coulomb gas

The classical Coulomb gas is given by the Hamiltonian

$$\mathcal{H}_{\rm CG}=\tfrac{1}{2}\sum_{i,j} q_i V(\mathbf{r}_i-\mathbf{r}_j)q_j \ , \tag{1}$$

where the sum is over all pairs of sites of a two-dimensional periodic $L\times L$ lattice. q_i is the charge at site i and $V(\mathbf{r})$ is the lattice Coulomb potential in two dimensions (2D), which solves the equation

$$\Delta^2 V(\mathbf{r})=-2\pi\delta_{\mathbf{r},0} \ . \tag{2}$$

Here Δ^2 is the discrete form of the Laplacian, which is defined as

$$\Delta^2 f(\mathbf{r})=c\sum_{\hat{\mu}}[f(\mathbf{r}+\hat{\mu})-2f(\mathbf{r})+f(\mathbf{r}-\hat{\mu})] \ , \tag{3}$$

where $\{\pm\hat{\mu}\}$ are the unit vectors from the site $\mathbf{r}$ to its nearest neighbors, and c is a geometrical factor which is required to get the correct form of the Laplacian in the continuum limit. We take periodic boundary conditions at the edges of the lattice. Here we will consider two cases; the square and triangular lattices. For the square lattice, $c=1$, and $\{\hat{\mu}\}=\{\hat{\mathbf{a}}_1,\hat{\mathbf{a}}_2\}$, where $\{\hat{\mathbf{a}}_1,\hat{\mathbf{a}}_2\}=\{\hat{\mathbf{x}},\hat{\mathbf{y}}\}$ are the unit basis vectors. For a triangular lattice, $c=\frac{4}{6}$, and $\{\hat{\mu}\}=\{\hat{\mathbf{a}}_1,\hat{\mathbf{a}}_2,\hat{\mathbf{a}}_3\}$, where $\{\hat{\mathbf{a}}_1,\hat{\mathbf{a}}_2\}=\{\hat{\mathbf{x}},\frac{1}{2}\hat{\mathbf{x}}+(\sqrt{3}/2)\hat{\mathbf{y}}\}$ are the unit basis vectors, and $\hat{\mathbf{a}}_3\equiv\hat{\mathbf{a}}_2-\hat{\mathbf{a}}_1$. Substituting the Fourier transforms

$$V(\mathbf{r})\equiv\frac{1}{N}\sum_{k} V_k e^{i\mathbf{k}\cdot\mathbf{r}} \ , \quad \delta_{\mathbf{r},0}=\frac{1}{N}\sum_{k} e^{i\mathbf{k}\cdot\mathbf{r}} \tag{4}$$

into Eq. (2), one finds for the square lattice

$$V_k=\frac{\pi}{2-\cos(\mathbf{k}\cdot\hat{\mathbf{a}}_1)-\cos(\mathbf{k}\cdot\hat{\mathbf{a}}_2)} \tag{5}$$

and for the triangular lattice

$$V_k=\frac{3\pi}{6-2\cos(\mathbf{k}\cdot\hat{\mathbf{a}}_1)-2\cos(\mathbf{k}\cdot\hat{\mathbf{a}}_2)-2\cos(\mathbf{k}\cdot\hat{\mathbf{a}}_3)} \ . \tag{6}$$

Here $N=L^2$ is the number of sites. The wave vectors used in the summations in Eq. (4) are determined by periodic boundary conditions, and given by $\{\mathbf{k}\}=\{(m_1/L)\mathbf{b}_1+(m_2/L)\mathbf{b}_2\}$, where $m_1,m_2=0,1,2,\ldots,L-1$, and $\{\mathbf{b}_i\}$ are the basis vectors of the reciprocal lattice. For the square lattice $\{\mathbf{b}_1,\mathbf{b}_2\}=\{2\pi\hat{\mathbf{x}},2\pi\hat{\mathbf{y}}\}$, and for the triangular lattice

$$\{\mathbf{b}_1,\mathbf{b}_2\}=\left\{2\pi\hat{\mathbf{x}}-\frac{2\pi}{\sqrt{3}}\hat{\mathbf{y}},\frac{4\pi}{\sqrt{3}}\hat{\mathbf{y}}\right\} \ .$$

From Eqs. (4–6), we see that $V(\mathbf{r})$ diverges due to the divergence of V_k as $\mathbf{k}\to 0$. To treat this infrared divergence, we decompose $V(\mathbf{r})$ into two pieces, $V(\mathbf{r})=V'(\mathbf{r})+V(\mathbf{r}=0)$, where

$$V'(\mathbf{r})\equiv V(\mathbf{r})-V(\mathbf{r}=0)=\frac{1}{N}\sum_{k} V_k(e^{i\mathbf{k}\cdot\mathbf{r}}-1) \tag{7}$$

is nonsingular. Substituting this decomposition into (1), the CG Hamiltonian can be written as

$$\mathcal{H}_{\rm CG}=\tfrac{1}{2}\sum_{i,j} q_i V'(\mathbf{r}_i-\mathbf{r}_j)q_j+V(0)\left[\sum_i q_i\right]^2 \ . \tag{8}$$

Since $V(0)$ is positive and infinite, the above implies that only the neutral configurations will contribute to the partition sum. So we wind up with the Hamiltonian

$$\mathcal{H}_{\rm CG}=\tfrac{1}{2}\sum_{i,j} q_i V'(\mathbf{r}_i-\mathbf{r}_j)q_j \ , \tag{9}$$

where the neutrality condition $\sum_i q_i=0$ is imposed and the nonsingular interaction V' is used. In our calculations, V' is explicitly evaluated using Eqs. (5–7).

In our work, we have considered two cases: the *integer* CG, and the *fractional* CG. For the integer CG, the charges take the integer values $q_i=0,\pm1,\pm2,\ldots$. We are interested in studying the dense limit of this model, so we introduce a chemical potential $-u$, which controls the average charge density of the system. In this case the Hamiltonian becomes

$$\mathcal{H}_{\rm CG}=\tfrac{1}{2}\sum_{i,j} q_i V'(\mathbf{r}_i-\mathbf{r}_j)q_j-u\sum_i q_i^2+\sum_i (q_i^4-q_i^2) \ . \tag{10}$$

Increasing u, at fixed temperature T, increases the average charge density. The third term has been added to stabilize the system in the very dense limit, as will be discussed later. We will find that, at small u (low densities), the ground state of (10) is the vacuum $q_i=0$. At higher $u>u_0$, the ground state will be an ordered charge lattice.

For the fractional CG, the charges take the fractional values

$$q_i=n_i-f \ , \tag{11}$$

where $n_i=0,\pm1,\pm2,\ldots$ is an integer, and f is a fixed constant $0<f<\frac{1}{2}$. The lowest magnitude charges are thus $1-f$ and $-f$, and $q_i=0$ is no longer allowed. We may view n_i as integer charges placed on a uniform background charge of $-f$. Neutrality leads to the constraint $\sum_i n_i=Nf$ or $\langle n_i\rangle=f$. In this case, we use the Hamiltonian (9) and the ground state consists of an ordered charge lattice.

The transitions of the Coulomb gas in which we are interested consist of two types. The first is the "metal-insulator" transition, where the dielectric constant ϵ of the charges diverges. The inverse dielectric constant, as given by standard linear response theory,[6,14] is

$$\epsilon^{-1}(T,L)=\lim_{k\to 0}\left\{1-\frac{2\pi}{k^2 TN}\langle q_k q_{-k}\rangle\right\} \ , \tag{12}$$

where

$$q_k \equiv \sum_i q_i e^{-i\mathbf{k}\cdot\mathbf{r}_i} \tag{13}$$

is the Fourier transform of the charge density. In our simulations, ϵ^{-1} is approximated by averaging over the two smallest allowed wave vectors for each system size. For the square lattice these are $(2\pi/L)\hat{\mathbf{x}}$, $(2\pi/L)\hat{\mathbf{y}}$, and for the triangular lattice these are $(2\pi/L)\hat{\mathbf{x}} - (2\pi/\sqrt{3}L)\hat{\mathbf{y}}$, $(4\pi/\sqrt{3}L)\hat{\mathbf{y}}$.

Secondly, we are interested in studying the melting transitions of the ordered charge lattices, which form in the ground state of the fractional, and very dense integer, Coulomb gases. Such transitions may be signaled by the divergence of the specific heat or order-parameter susceptibility. We wish to investigate whether standard symmetry analysis can predict the universality of these transitions, despite the fact that the Coulomb interactions of our model are long range.

B. Monte Carlo algorithm

In order to investigate the phase diagram of the Coulomb gas models described above, we use Monte Carlo (MC) simulations. At each step of the simulation we pick a pair of nearest-neighbor sites (i_0,i_1) at random and add a unit charge to site $i_0, \Delta q_{i_0} = +1$, and subtract a unit charge from site i_1, $\Delta q_{i_1} = -1$. This excitation is then either accepted or rejected using the standard Metropolis algorithm

$$\text{accept if } e^{-\Delta E/T} > r \ , \tag{14}$$

where r is a random number uniformly distributed on the interval [0,1), and

$$\Delta E = E_{\text{new}} - E_{\text{old}} \tag{15}$$

is the change in energy due to the addition of the excitation.

As the interactions between charges are long range, the evaluation of ΔE can be time consuming. Considering only the Coulomb interaction piece of the Hamiltonian, given in Eq. (9) (i.e., ignoring the chemical potential term we add for the integer CG), we may write ΔE as

$$\Delta E = \sum_{i=i_0,i_1;j} [\Delta q_i V'(\mathbf{r}_i - \mathbf{r}_j) q_j] + \Delta q_{i_0} V'(\mathbf{r}_{i_0} - \mathbf{r}_{i_1}) \Delta q_{i_1} \ , \tag{16}$$

where we have used the fact that $V'(\mathbf{r}) = V'(-\mathbf{r})$ and $V'(0) = 0$. In this form, each evaluation of ΔE is a computation of order N, as j sweeps the entire lattice. To speed this process up, we use an algorithm given by Grest.[14] In analogy to electrostatics, we define the total potential at site i by

$$F_i = \sum_j V'(\mathbf{r}_i - \mathbf{r}_j) q_j \ . \tag{17}$$

Now each evaluation of

$$\Delta E = \Delta q_{i_0} F_{i_0} + \Delta q_{i_1} F_{i_1} + \Delta q_{i_0} V'(\mathbf{r}_{i_0} - \mathbf{r}_{i_1}) \Delta q_{i_1} \tag{18}$$

requires computation of only $O(1)$. To implement this method, it is necessary to update the F_i, $i = 1, \ldots, N$, each time the charge configuration changes, i.e., each time an excitation is accepted:

$$F_{i,\text{new}} = F_{i,\text{old}} + V'(\mathbf{r}_i - \mathbf{r}_{i_0}) \Delta q_{i_0} + V'(\mathbf{r}_i - \mathbf{r}_{i_1}) \Delta q_{i_1} \ . \tag{19}$$

For updating N such variables, the computation is of order N. However, as this computation need only be done when an excitation is accepted, when the acceptance rate is low, this method is substantially faster than the direct approach of Eq. (16).

$N = L^2$ steps of this process of updating the configurations will be referred to as one MC pass. At each temperature, an initial 10 000 passes are typically discarded to equilibrate the system. The final configuration after equilibration is then saved. To compute averages, we perform five independent runs, each starting from this saved configuration, but using different random number sequences. Error bars are estimated from the standard deviation of the averages from these five runs. In most cases, 200 000 passes were used to calculate the averages of each of these five runs.

C. Finite-size-scaling analysis

To determine transition temperatures T_c, and calculate critical exponents, we apply finite-size-scaling analysis[19–22] to the results of our Monte Carlo simulations. We summarize these finite-size-scaling methods below.

We first consider the charge lattice melting transitions, for which there is a well-defined intensive order parameter $M > 0$, at low temperatures. M will typically be a particular Fourier component of the charge density. If the reduced temperature is $t = (T - T_c)/T$, the system length is L, and h is the ordering field conjugate to M, then the singular part of the free-energy density, $f \equiv L^{-d} \ln Z$, near the critical point $(T_c, h = 0, 1/L = 0)$, obeys the scaling relation[19,20]

$$f_s(t,h,L) = b^{-d} f_s(t b^{y_t}, h b^{y_h}, L/b) \ , \tag{20}$$

where b is the rescaling factor, d the dimensionality of the system, and y_t and y_h are the eigenvalues of the renormalization transformation for the scaling fields t and h. The finite-size-scaling behavior of the specific-heat density, at $h = 0$, is then given by setting $b = L$, and differentiating

$$\begin{aligned} C(T,L) &= -\frac{1}{T^2} \frac{\partial^2 f}{\partial K^2} \\ &= -L^{2y_t - d} \left[\frac{T_c}{T} \right]^2 f_{tt}(t L^{y_t}, 0, 1) + \phi_C(t,L) \ , \end{aligned} \tag{21}$$

where $K \equiv 1/T$, f_{tt} is the second derivative of f_s with respect to t, and ϕ_C is the contribution from the nonsingular part of the free energy f. Within our simulation, C is computed by the usual fluctuation formula

$$C = \frac{1}{L^d T^2} (\langle \mathcal{H}_{\text{CG}}^2 \rangle - \langle \mathcal{H}_{\text{CG}} \rangle^2) \ . \tag{22}$$

Similarly, the order-parameter susceptibility, at $h=0$, is given by

$$\chi_M \equiv \left.\frac{\partial M}{\partial h}\right|_{h=0} = \left.\frac{\partial^2 f}{\partial h^2}\right|_{h=0} = L^{2y_h-d} f_{hh}(tL^{y_t},0,1) , \tag{23}$$

where f_{hh} is the second derivative of f_s with respect to h. Since the field h couples to M only in the very long-wavelength limit ($\mathbf{k}\to 0$), we can choose[23] to include all the h dependences of the free energy in the singular part f_s, and hence there is no nonsingular contribution to χ_M, as there is to C. χ_M is computed within our simulation by the fluctuation formula

$$\chi_M = \frac{L^d}{T}(\langle M^2\rangle - \langle M\rangle^2) . \tag{24}$$

Since for any finite-size system L the order parameter vanishes, $\langle M\rangle = 0$, Eqs. (23) and (24) result in the scaling law for the order parameter squared,

$$M^2 = T\frac{\chi_M}{L^d} = L^{2(y_h-d)} T f_{hh}(tL^{y_t},0,1) . \tag{25}$$

From Eqs. (21), (23), and (25) we identify

$$\begin{aligned} 1/\nu &= y_t , \\ \alpha/\nu &= 2y_t - d , \\ \gamma/\nu &= 2y_h - d , \end{aligned} \tag{26}$$

and

$$\beta/\nu = d - y_h ,$$

where ν, α, γ, and β, are the usual critical exponents of the correlation length, specific heat, susceptibility, and magnetization, respectively. Implicit in Eq. (26) are the familiar hyperscaling, $\alpha = 2-d\nu$, and Rushbrook, $\alpha+2\beta+\gamma=2$, results.[24]

To apply these finite-size-scaling results to extract critical behavior from Monte Carlo data, we first consider a method used by Barber and Selke.[21] If $A(T,L)$ is some thermodynamic quantity, which obeys the finite-size-scaling relation

$$A(T,L) \sim L^x \Phi(tL^{y_t}) , \tag{27}$$

we form the ratio

$$R_A(T;L,L') \equiv \frac{A(T,L)}{A(T,L')} = \left[\frac{L}{L'}\right]^x \frac{\Phi(tL^{y_t})}{\Phi(t[L']^{y_t})} \tag{28}$$

using data from two different system sizes L and L'. From Eq. (28) we see that different curves of $R_A(T;L,bL)$ and $R_A(T;L',bL')$ vs T should all intersect only at T_c ($t=0$), where R_A has the common value b^x. From this common intersection point, we can thus estimate both T_c and the scaling exponent x. This method can work well only when the nonsingular contribution to A vanishes, or when the singular part diverges fast enough with L, so as to make the nonsingular contribution negligible. It thus should be good when applied to χ_M (provided L is large enough to be in scaling region), but might be problematic when applied to C, if C is only weakly divergent (as in a 2D Ising transition, for example).

The above method can determine the correlation length exponent $\nu = 1/y_t$, only through the hyperscaling relation $\alpha/\nu = 2/\nu - d$, with α/ν determined from R_C. Since this ratio method may not work well for C, it is useful to have a more direct method for extracting ν from the Monte Carlo data. Such a scheme was given by Nightingale and Blöte.[22] Taking the scaling form for the order parameter squared, Eq. (25), we can expand the scaling function f_{hh} about T_c, where $tL^{1/\nu}$ is small:

$$M^2(T,L) = L^{-2\beta/\nu}[\Phi_0 + \Phi_1 L^{1/\nu}(T-T_c) + O(L^{2/\nu}(T-T_c)^2)] . \tag{29}$$

Truncating this expansion at any finite order, we can do a least χ^2 fit of the data $M^2(T,L)$ to determine the unknown parameters $2\beta/\nu$, $1/\nu$, T_c, Φ_0, etc. As the scaling form (29) applies only at sufficiently large L, we may check that we have reached this scaling limit by dropping data from the smallest size L and repeating the fit. We continue this process, dropping data from the successively lowest sizes L, until the parameter values we obtain do not vary within the estimated error when either the next lowest L data is dropped or the expansion is continued to the next order. To estimate the errors in the fitted parameters, we generate many synthetic data sets by adding random noise to each of the original MC data points. The noise for each data point is taken from a Gaussian distribution whose width is set equal to the estimated statistical error of the original MC data point. Using these fictitious data sets, we repeat the fitting procedure to obtain new values of the parameters. The estimated error of a parameter is then taken as the standard deviation of the results from all the fictitious data sets. For our fitting, we use the Levenberg-Marquart method.[25]

The above discussion will be applied to the charge lattice melting transitions of the CG. We now return to the "metal-insulator" transition. The Kosterlitz-Thouless argument,[2] viewed as an instability criteria, shows that neutral bound pairs of charges will unbind, driving $\epsilon^{-1}\to 0$, when $\epsilon^{-1}(T) < 4T$. In the KT analysis, this holds as an equality at the transition T_c. More generally, however, we can view it as giving an upper bound on T_c,

$$T_c < \epsilon^{-1}(T_c,L)/4 . \tag{30}$$

Thus, there is a discontinuous jump to zero in ϵ^{-1} at the transition. For a more precise location of T_c we use finite-size scaling. Using the mapping[6,7] between the inverse dielectric constant, and the helicity modulus of the corresponding XY model, we expect the finite-size-scaling behavior of ϵ^{-1} at T_c to be given by the Josephson relation[26]

$$\epsilon^{-1}(T,L) \sim L^{2-d} H(L/\xi(T)) , \tag{31}$$

where ξ is the correlation length, and $\xi\to\infty$ at T_c. For $d=2$, we thus might expect that $\epsilon^{-1}(T_c,L)$ is independent of L, i.e., curves of ϵ^{-1} vs T, for different L, would

all intersect at the same point T_c. For the KT transition, however, a more detailed finite-size analysis by Weber and Minnhagen,[27] based on the Kosterlitz recursion equations, finds a logarithmic correction to the scaling behavior at T_c. They find,

$$\epsilon^{-1}(T_c,L)=\epsilon_\infty^{-1}\left[1+\frac{1}{2\ln L+c}\right], \tag{32}$$

where, for the KT transition, we have the universal result $\epsilon_\infty^{-1}\equiv\epsilon^{-1}(T_c,\infty)=4T_c$. To determine the transition temperature of the "metal-insulator" transition, and the jump in ϵ^{-1} at this transition, we follow Weber and Minnhagen's approach. We do a least χ^2 fit of the Monte Carlo data at all temperatures, to the form (32) with ϵ_∞^{-1} and c as free parameters. The temperature at which the χ^2 is smallest, we identify as the transition T_c, and the fitted parameter ϵ_∞^{-1} gives the jump in the inverse dielectric constant.

III. THE INTEGER COULOMB GAS ON A SQUARE LATTICE

A. Phase diagram

Our results for the integer Coulomb gas on a square lattice, using the Hamiltonian (10), are summarized by the u-T phase diagram shown in Fig. 1. Phase $\mathcal{A}$, at small u and T, is qualitatively the same as the low-temperature phase in the Kosterlitz-Thouless model. The ground state is the vacuum, and at finite T, charge excitations exist as bound neutral clusters. The dielectric constant $\epsilon^{-1}>0$, and the system is insulating. As T increases within $\mathcal{A}$, there is a "metal-insulating" transition (dashed line) to a conducting phase $\mathcal{B}$, where ϵ^{-1} vanishes. As u increases at small T within $\mathcal{A}$, there is a first-order transition (thick solid line) to an insulating phase $\mathcal{D}$. In $\mathcal{D}$ the ground state is an ordered checkerboard lattice of $+1,-1$ charges, which is doubly degenerated and characterized by an Ising-like order parameter M (analogous to the staggered magnetization of an Ising antiferromagnet). As T increases within $\mathcal{D}$, there is first a "metal-insulator" transition (dashed line) to a conducting phase $\mathcal{E}$, with vanishing ϵ^{-1}, however, a nonvanishing order parameter $M\neq 0$. This is followed at higher temperatures by a charge lattice melting transition (thin solid line) to phase $\mathcal{B}$, where $M=0$. This combination of "metal-insulator" transition and lattice melting transition is reminiscent of behavior in the fully frustrated XY model[8,13] [or, equivalently, the $f=\frac{1}{2}$ fractional CG (Ref. 14)]. However, as opposed to that model, here we find a clear separation between the two transitions. The first order (thick solid) line between $\mathcal{A}$ and $\mathcal{D}$ meets the second order (thin solid) line between $\mathcal{E}$ and $\mathcal{B}$ at point $\mathcal{C}$. The "metal-insulator" (dashed) lines meets the first-order (thick solid) line at a temperature *below* point $\mathcal{C}$. The "metal-insulator" transitions obey the universal Kosterlitz-Thouless behavior. The lattice melting transition is Ising-like. Point $\mathcal{C}$ appears to be a multicritical point.

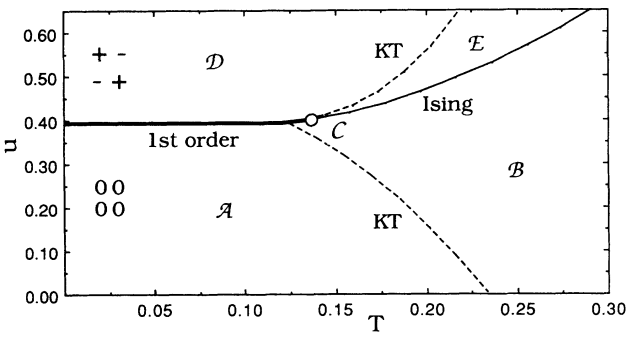

FIG. 1. Phase diagram for the classical neutral integer charge 2D Coulomb gas on a square lattice as a function of temperature T and parameter u. Increasing u increases the average charge density. The dashed lines are Kosterlitz-Thouless transitions where the dielectric function ϵ diverges. The thick solid line is a first-order transition to a charge lattice ground state. The thin solid line is an Ising-like second-order transition at which the charge lattice melts. $\mathcal{C}$ is a tricritical point where the Ising and first-order lines meet. The KT lines meet the first-order line at a temperature *below* $\mathcal{C}$.

B. First-order transition

The first-order line in Fig. 1 is easily explained by considering the ground state of the system as u is increased. Taking the Fourier transform of the first two terms in the Hamiltonian (10) gives

$$\mathcal{H}_{\rm CG}=(1/N)\sum_k(\tfrac{1}{2}V_k-u)|q_k|^2, \tag{33}$$

where V_k is given in Eq. (5) and q_k in Eq. (13). The minimum value of the Coulomb potential V_k occurs at the wave vector $\mathbf{k}_0=\pi\hat{\mathbf{x}}+\pi\hat{\mathbf{y}}$, where $V_{k_0}=\pi/4$. When $u<\frac{1}{2}V_{k_0}=\pi/8=0.392\,699\equiv u_0$, then $\frac{1}{2}V_k-u>0$ for all $\mathbf{k}$ and hence the ground state of the system will be the vacuum, with all $q_k=0$ (phase $\mathcal{A}$). However, for $u>u_0$, the system will lower its energy by ordering in a state with nonzero q_{k_0}. This state will be a checkerboard pattern of alternating positive and negative charges of equal magnitude (see inset to phase $\mathcal{D}$ in Fig. 1). If the Hamiltonian had only the terms as in Eq. (33), then, since the charges q_i can take any integer value, the system would be unstable for $u>u_0$, with the magnitude of each $|q_i|$ growing without bound. This therefore motivates the inclusion of the third term in the Hamiltonian (10), $\sum_i(q_i^4-q_i^2)$. This term suppresses charges $|q_i|>1$ and thus stabilizes the system for some finite interval of $u>u_0$ into a checkerboard pattern of ±1 charges (for sufficiently large u, a ±2 charge pattern would become the ground state). This discontinuous change in the ground state, from the vacuum to an ordered charge lattice at $u_0=\pi/8$, extends into a first-order transition line at finite T.

C. Charge lattice melting transition

Having demonstrated the existence of the charge lattice ground state, for $u>u_0$, we now find the boundaries

of this phase. The order parameter describing this phase is

$$M \equiv \frac{1}{N}\langle q_{k_0}\rangle = \frac{1}{N}\sum q_i(-1)^{\mathbf{r}_i\cdot(\hat{\mathbf{x}}+\hat{\mathbf{y}})}, \tag{34}$$

where $\mathbf{k}_0=\pi\hat{\mathbf{x}}+\pi\hat{\mathbf{y}}$ is the ordering wave vector. M is analogous to the "staggered magnetization" of an Ising antiferromagnet. From symmetry, we expect that this charge lattice will melt with a second-order Ising-like transition, as temperature is increased. This line of melting transitions (thin solid line in Fig. 1) is located by observing the finite-size-scaling behaviors of the specific heat C and order parameter M. For the Ising transition in two dimensions, it is known that $\alpha=0$, and hence the specific heat scales logarithmically with size,[19] $C(T_c)\sim \ln L$.

An example of our results is shown in Fig. 2(a), in which we plot the peak value of $C(T)$ for each L vs $\ln L$ at $u=0.5$ and find linear scaling consistent with Ising behavior. The same behavior was also found for the values $u=0.45$ and 0.6. As an independent test that this melting transition is Ising-like, we also consider the scaling behavior of the order parameter squared, M^2. For $u=0.5$, our data is shown in Fig. 2(b). To determine the critical exponents, we fit M^2 to the expansion Eq. (29), using the procedure outlined in Sec. II C. Using a second-order expansion of Eq. (29), the results obtained from the data for sizes $L=10$, 12, and 16, give the values $T_c=0.2205\pm0.0019$, $1/\nu=1.01\pm0.13$, $\beta/\nu=0.130\pm0.033$. The exact exponents for the 2D Ising model are, $1/\nu=1$, $\beta/\nu=\frac{1}{8}$. In Fig. 2(b), the solid lines are plotted from Eq. (29) using the fitted values of the parameters. Similarly, the exponents used in the scaling of the axes come from our fit.

In contrast to the Ising behavior described above, a more divergent behavior is observed at $u=0.4$, as T varies through point $\mathcal{C}$. In Fig. 3(a), a plot of the specific-heat maximum, $\ln C_{\max}$ vs $\ln L$ indicates a power-law divergence of $\alpha/\nu\simeq 1.16$, which from Eq. (26) gives $1/\nu=1.58$. This suggests that $\mathcal{C}$ is a tricritical point at which the line of second-order Ising transitions meets the first-order transition line between phases $\mathcal{A}$ and $\mathcal{D}$. To describe the scaling behavior near a tricritical point, one needs two relevant scaling fields, in contrast to an ordinary second-order critical point where there is only one. Let $g_1(T,u)$ and $g_2(T,u)$ be the two scaling fields which give the most and next most relevant directions in the u-T plane. At the tricritical point, $g_{1,2}(T_c,u_c)=0$. The line in the u-T plane where $g_2=0$ defines the "g_1 direction." The line where $g_1=0$ defines the "g_2 direction." The g_2 direction is generally believed to lie parallel to the second-order phase boundary.[28] The scaling of the free energy near a tricritical point is then given by[28]

$$f_s(g_1,g_2,h,L)=L^{-d}f_s(g_1L^{y_1},g_2L^{y_2},hL^{y_h},1), \tag{35}$$

where y_1 and y_2 are the eigenvalues of the scaling field g_1 and g_2, and $y_1>y_2>0$. Assuming that the T axis at $\mathcal{C}$ has a nonzero projection onto the g_1 direction, we have, for the leading finite-size-scaling behavior of the specific heat,

$$C(L)\sim L^{2y_1-d}f_{11}(g_1L^{y_1},g_2L^{y_2},hL^{y_h},1), \tag{36}$$

where f_{11} is the second derivative of f_s with respect to g_1. Similarly, if the u axis at $\mathcal{C}$ has a nonzero projection onto the g_1 direction, then the charge density susceptibility

$$\chi_q \equiv -T\frac{\partial^2 f}{\partial u^2} = \frac{1}{NT}\left\{\left\langle\left[\sum_i q_i^2\right]^2\right\rangle-\left\langle\sum_i q_i^2\right\rangle^2\right\} \tag{37}$$

should have the same leading scaling behavior as the specified heat C in Eq. (36), $\chi_q(T_c)\sim L^{2y_1-d}$. We define this leading exponent $2y_1-d\equiv\alpha/\nu$.

To test this scaling behavior, we apply the method of

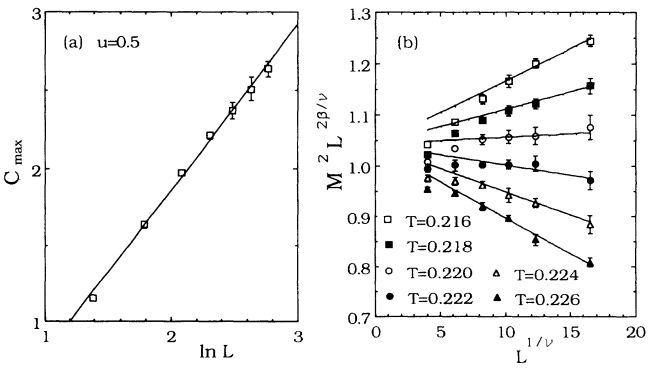

FIG. 2. (a) $C_{\max}$ vs $\ln L$ at $u=0.5$. $C_{\max}\sim\ln L$ indicates an Ising transition. (b) The finite-size-scaling behavior of the order parameter M^2 at $u=0.5$. Symbols with error bars represent the MC data. The solid lines represent the result of fitting Eq. (29) to a second-order expansion in $T-T_c$, using data from $L=10$–16. The fitted values of $1/\nu=1.0120$ and $\beta/\nu=0.1299$ were used in making the axes of the plot. 750 000 total MC passes were used.

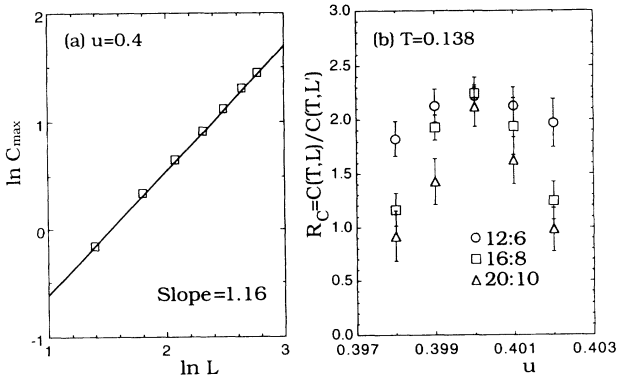

FIG. 3. (a) $\ln C_{\max}$ vs $\ln L$ at $u=0.4$ passing through point $\mathcal{C}$ (see Fig. 1). (b) Ratio of specific heats R_C along a trajectory perpendicular to the phase boundary (see Fig. 1) passing through point $\mathcal{C}$. Three different sets of lattice lengths L:L' with the same ratio 2 are shown. The common intersection of the three curves is at $(u_c,2^{\alpha/\nu})$. 10^6 total MC passes were used.

Sec. II C to our data, and compute the ratios $R_C \equiv C(L)/C(L')$ and $R_{\chi_q} \equiv \chi_q(L)/\chi_q(L')$ [see Eq. (28)], as we vary the parameter u along a trajectory passing through point $\mathcal{C}$ perpendicular to the phase boundary. In Fig. 3(b), we plot R_C for ratios $L/L' = \frac{12}{6}, \frac{16}{8}$, and $\frac{20}{10}$. The three curves do indeed intersect at a single point ($u_c = 0.4$, $T_c = 0.138$), with $R_c(u_c) = 2^{\alpha/\nu} = 2.15 \pm 0.25$, thus giving $\alpha/\nu = 2y_1 - d = 1.10 \pm 0.16$. Since $d = 2$, we have $y_1 \equiv 1/\nu = 1.55 \pm 0.08$. A similar analysis[18(a)] of R_{χ_q} gives consistent values of $\alpha/\nu = 1.14 \pm 0.2$ and, hence, $1/\nu = 1.57 \pm 0.10$.

The quantities

$$-C/T^2 = (1/T^4)\partial^2 f/\partial K^2 = \partial^2 f/\partial T^2$$

(to leading order as $L \to \infty$, at point $\mathcal{C}$) and $-\chi_q/T = \partial^2 f/\partial u^2$ represent second derivatives of the free energy f in the particular directions T and u. Similarly we can compute the second derivative $f_{ee} \equiv (\hat{\mathbf{e}} \cdot \nabla)^2 f$ along *any* direction $\hat{\mathbf{e}}$ in the u-T plane. At the tricritical point (T_c, u_c), to leading order as $L \to \infty$,

$$-f_{ee} = \frac{C + s^2 T \chi_q + (2s/NT)[\langle \mathcal{H}_{CG} \sum_i q_i^2 \rangle - \langle \mathcal{H}_{CG} \rangle \langle \sum_i q_i^2 \rangle]}{T^2(1+s^2)}, \tag{38}$$

where $s \equiv du/dT$ is the slope of the unit vector $\hat{\mathbf{e}}$. At the tricritical point, f_{ee} will grow fastest with increasing L when $\hat{\mathbf{e}}$ lies along the most relevant direction g_1. Computing this general f_{ee} as in Eq. (38), at the tricritical point (T_c, u_c) located by the ratio analysis above, and varying $\hat{\mathbf{e}}$, we determine that the g_1 direction lies perpendicular to the phase boundary, while g_2, the direction of slowest growth, lies along the phase boundary. In Fig. 4, we show $f_{ee}(T_c, u_c)$ for these two directions vs L. The approximate linear divergence in the g_1 direction agrees with our previous results from C and χ_q, but the data in the g_2 direction are not accurate enough to estimate the next most relevant exponent y_2.

We now find the order-parameter exponent β/ν by computing the square of the order parameter $M^2(T,u,L)$ along the direction g_1 as determined above. Since $g_2 = 0$ along this trajectory, M^2 has the scaling form

$$M^2 = L^{-2\beta/\nu} f_{hh}(g_1(T[u],u)L^{1/\nu}, 0, 0, 1) \tag{39}$$

with $g_1(T[u],u) \sim (u - u_c)$ close to the tricritical point. Expanding the scaling function f_{hh} in powers of $(u - u_c)L^{y_1}$, we get a form analogous to Eq. (29), to which we fit our data in order to estimate the exponents β/ν and $1/\nu$. We show the results of this fitting in Table I as a typical example to illustrate the accuracy of the fit.[29] Using a fourth-order expansion in $u - u_c$ for the sizes $L = 10$–16, we find the best fit to yield[30] $\beta/\nu = 0.08 \pm 0.04$, $1/\nu = 1.67 \pm 0.08$, and $u_c = 0.4 \pm 0.0003$, giving agreement for $1/\nu$ and u_c with the values found in the ratio analysis of C and χ_q.

With respect to the charge lattice ordering, the Hamiltonian (10) has the same symmetry as an antiferromagnetic Blume-Emery-Griffiths model.[31] One might therefore expect that point $\mathcal{C}$ is an Ising tricritical point, in which case the exact exponents[28] would be $\alpha/\nu = 1.6$, $\beta/\nu = 0.075$. This value for α/ν is distinctly different from our finite-size-scaling result. We thus believe that point $\mathcal{C}$ may not be the usual Ising tricritical point.

D. Metal-insulator transition

Finally, we consider the "metal-insulator" transitions (dashed lines in Fig. 1). Crossing from phase $\mathcal{A}$ to $\mathcal{B}$, below the first-order line, we observe that the specific-heat peak saturates to a finite value as L is increased. Such behavior is characteristic of the KT transition, in which the free energy has only a weak essential singularity at T_c, and the peak in C occurs slightly above T_c.[19,32] As a better indicator of the transition, we consider the inverse dielectric constant ϵ^{-1} defined in Eq. (12). In Fig. 5, we plot $\epsilon^{-1}(T)$ for the fixed size $L = 12$, for several values of u both below and above the first-order line. The intersection of the curves of ϵ^{-1} with the dashed line, $4T$, gives an estimate for the upper bound on the transition, according to the KT instability argument, Eq. (30). Thus we locate the "metal-insulator" phase boundaries shown in Fig. 1 (dashed lines). In Fig. 6, we plot ϵ^{-1} vs u, for $L = 12$, at the fixed value of $T = 0.135$ which is lower than the tricritical point $\mathcal{C}$ at $T_c = 0.138$. The minimum of $\epsilon^{-1}(u)$ lies at $u \simeq 0.394 \simeq u_0 = \pi/8$ and locates the position of the phase boundary between $\mathcal{A}$ and $\mathcal{D}$. The curve of $\epsilon^{-1}(u)$ is seen to lie below the dashed line, $4T$, for the interval $0.372 < u < 0.40$. Using the KT bound, Eq. (30), we conclude that the "metal-insulator" transitions for u in this interval lie at temperatures lower than $T = 0.135$, i.e., the "metal-insulator" transition lines in Fig. 1 meet the first-order transition line at a temperature *below* the tricritical point $\mathcal{C}$.

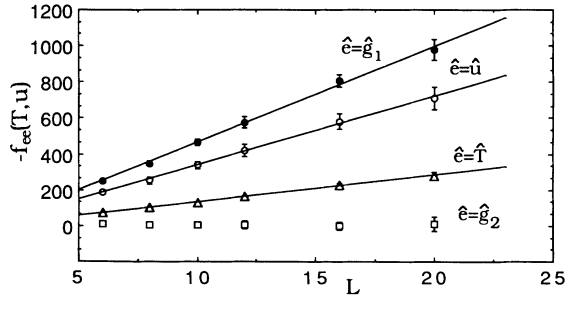

FIG. 4. Second derivative of the free energy $f(T,u)$, in the direction $\hat{\mathbf{e}}$, evaluated at point $\mathcal{C}$ vs square lattice length L. The direction $\hat{\mathbf{g}}_1$ of the most rapid growth with L locates the most relevant scaling direction, which was found to be perpendicular to the phase boundary. Approximately linear scaling $f_{ee} \sim L$ is found for all but the $\hat{\mathbf{g}}_2$ direction parallel to the phase boundary.

TABLE I. Results for the fitting of M^2 to the expanded form of the scaling Eq. (39), analogous to Eq. (29), at point $\mathcal{C}$ of the square lattice. Fitting to a third- and a fourth-order expansion in $L^{y_1}(1/u-1/u_c)$ is shown. The first column shows the sequence of L for which the fitting is performed. The following columns give fitted parameters. Φ_i's are the coefficients of the ith order polynomial in $L^{y_1}(1/u-1/u_c)$. The last column is the $\chi^2_{\rm fit}$ error of the fit. Any $\chi^2_{\rm fit}$ which is of the order of the number of data points used in the fit indicates a good fit. For each sequence of L, the first row gives the value of the fitted parameter, while the second row gives the estimated error.

L_i-L_f	β/ν	$1/u_c$	$1/\nu$	Φ_0	Φ_1	Φ_2	Φ_3	Φ_4	$\chi^2_{\rm fit}$
				Third-order expansion					
8–16	0.0450	2.499	1.569	0.6831	−0.4547	−0.0680	0.1044		10.6
	0.0120	0.001	0.085	0.0256	0.0759	0.0368	0.0638		
10–16	0.0875	2.500	1.695	0.8057	−0.4160	−0.0202	0.0466		3.9
	0.0245	0.008	0.119	0.0808	0.0890	0.0157	0.0281		
12–16	0.0684	2.499	1.523	0.7463	−0.5858	−0.0655	0.1566		2.7
	0.0420	0.001	0.163	0.1632	0.2126	0.0245	0.1391		
				Fourth-order expansion					
8–16	0.0068	2.496	1.448	0.5727	−0.4747	−0.1207	0.3634	−0.1901	6.5
	0.0307	0.002	0.077	0.0545	0.1017	0.3317	1.4000	1.6000	
10–16	0.0790	2.500	1.672	0.7807	−0.4212	−0.0236	0.0538	−0.0016	3.5
	0.0415	0.002	0.077	0.1390	0.0870	0.0317	0.0280	0.0178	
12–16	0.0615	2.499	1.501	0.7268	−0.5967	−0.0642	0.1831	−0.0230	2.6
	0.0147	0.001	0.085	0.0488	0.2160	0.1153	0.1464	0.6903	

To test if these "metal-insulator" transitions belong to the Kosterlitz-Thouless universality class, we now consider the finite-size-scaling behavior of ϵ^{-1}. In Fig. 7, we plot $\epsilon^{-1}(T,L)$ at values $u=0.38$ just below the first-order line, and $u=0.4$ just above the first-order line. Following the discussion in Sec. II C by Eq. (31), a crude estimate of T_c is given by the temperature at which the curves of ϵ^{-1} for different L all intersect. We see that, at both values of u considered, this common intersection point occurs close to the KT bound on T_c given by (30), which in Fig. 7 is located by the intersection of ϵ^{-1} with the dashed line, $4T$.

For a more detailed finite-size-scaling approach, we do a least χ^2 fit, $\chi^2_{\rm fit}$, of $\epsilon^{-1}(L)$ to the expression Eq. (32), with c and ϵ_∞^{-1} as free parameters. The temperature at which $\chi^2_{\rm fit}$ is minimum we take as T_c, and the fitted ϵ_∞^{-1} gives the jump in ϵ^{-1} at T_c. In Fig. 8 we plot $\chi^2_{\rm fit}$, and the fitted ϵ_∞^{-1}/T vs T, using different ranges of lattice sizes L, for the same values of u as in Fig. 7. We see that, in both cases, the minimum of $\chi^2_{\rm fit}$ lies slightly above the temperature where the fitted ϵ_∞^{-1} equals the KT prediction, $4T_c$ (given by the intersection with the dashed line). This would imply a *smaller* than universal jump in $\epsilon^{-1}(T_c)$, inconsistent with the KT bound. Due to the considerable scatter in the curves for $\chi^2_{\rm fit}$, we conclude that this discrepancy is most likely a result of statistical inaccuracies in our data, and that there is no strong reason to suspect that the transitions are other than the universal KT type.

E. Nonzero ordering field

The resemblance of the phase diagram Fig. 1, to systems with Ising tricritical behavior, motivates us to con-

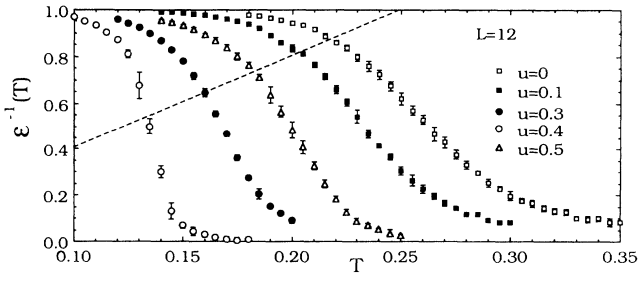

FIG. 5. Inverse dielectric function $\epsilon^{-1}(T)$ for fixed square lattice size $L=12$ for various values of u both below and above the first-order line at $u_0=\pi/8$. The intersection of the curves with the dashed line $4T$ gives the KT bound on T_c. 60 000 total MC passes were used.

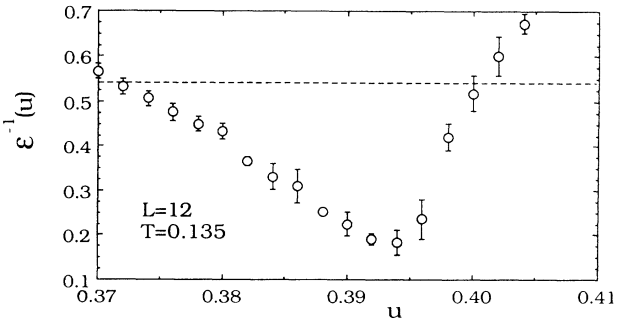

FIG. 6. Inverse dielectric function $\epsilon^{-1}(u)$ at constant $T=0.135$ for fixed square lattice size $L=12$. Points below the dashed line $4T$ are in the metallic phase according to the KT bound, Eq. (30). 60 000 total MC passes were used.

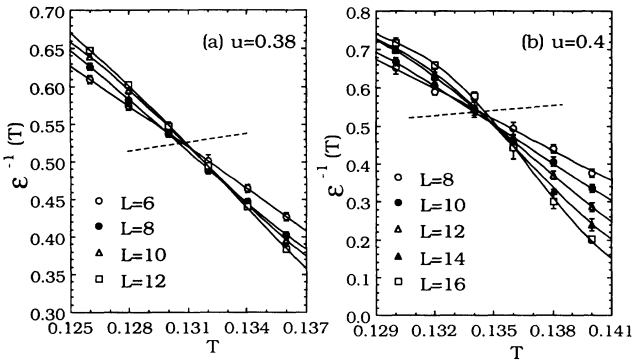

FIG. 7. Inverse dielectric function $\epsilon^{-1}(T)$ for constant (a) $u=0.38$ (just below the first-order line) and (b) $u=0.4$ (just above the first-order line) for various square lattice sizes L. The common intersection of the curves for different L approximates T_{KT}. The intersection with the dashed line $4T$ gives the KT upper bound $\epsilon^{-1}(T_c^-)\geq 4T_c$. 10^6 total MC passes were used.

sider the behavior of the Coulomb gas in a nonzero ordering field h which couples to the charge lattice order parameter M. We thus add to the Hamiltonian (10) the extra term

$$\delta\mathcal{H}_{CG}=-h\sum_i q_i(-1)^{\mathbf{r}_i\cdot(\hat{\mathbf{x}}+\hat{\mathbf{y}})}$$
$$=-h\langle q_{\mathbf{k}_0}\rangle=-hMN\ . \tag{40}$$

In the enlarged h-u-T phase space, the region of the $h=0$ symmetry plane containing phases $\mathcal{D}$ and $\mathcal{E}$ becomes a first-order surface across which there is a finite jump in M, from $M<0$ to $M>0$ as one varies h from negative to positive. We expect to find two additional first-order surfaces ("tricritical wings"), at $h>0$ and $h<0$, which meet and join this first-order symmetry surface at the first-order line in Fig. 1. This line is now a "triple line," as three distinct phases, $M>0$, $M<0$, $M=0$, coexist there. The tricritical wings are terminated by second-order critical lines which meet the second-order lattice melting line in Fig. 1 at the tricritical point $\mathcal{C}$ which ends the triple line.

In Fig. 9, we show the resulting phase diagram for (a) the $T=0$ plane, and (b) the plane for fixed $h=0.3$. In Fig. 9(a), the heavy solid lines are first-order transitions, across which there is a discontinuous jump in M. We can determine the locations of these lines, as in Sec. III B, by considering the Fourier transform of the Hamiltonian

$$\mathcal{H}_{CG}=\frac{1}{N}\sum_k(\tfrac{1}{2}V_k-u)|q_k|^2-hq_{\mathbf{k}_0}+\sum_i(q_i^4-q_i^2)\ , \tag{41}$$

where V_k is minimum at $\mathbf{k}_0$. The energy for the system to be in the charge lattice checkerboard configuration, with $\langle q_{\mathbf{k}_0}\rangle=\pm N$ $(M=\pm 1)$, is therefore $E/N=\frac{1}{2}V_{\mathbf{k}_0}-u-\mathrm{sgn}(h)h$, which becomes lower than the vacuum state with $E=0$ when

$$u>u_0(h)=u_0-\mathrm{sgn}(h)h\ , \tag{42}$$

where

$$u_0=\tfrac{1}{2}V_{\mathbf{k}_0}=\pi/8\ .$$

Equation (42) locates the diagonal lines in Fig. 9(a), while the vertical line is just the $h=0$ symmetry plane. The open circle where the three-order lines meet is the intersection of the triple line with the $T=0$ plane.

In Fig. 9(b), at $h=0.3$, $M>0$ everywhere at finite T. The first-order line (thick solid line) is the intersection of the tricritical wing with the $h=0.3$ plane. It is located at $T=0$ by Eq. (42), at $u_0(h=0.3)=0.092\,699$, and from our Monte Carlo results appears perfectly flat at higher temperatures. This line, across which there is a jump in M, from the dense phase $\mathcal{D}_+$ (large M), to the dilute phase $\mathcal{A}$ (small M), ends at a second-order Ising-like critical point I. The insulating phases $\mathcal{A}$ and $\mathcal{D}_+$ have "metal-insulator" transitions (dashed lines) to the conducting phase $\mathcal{B}$, which are of the KT type.

To demonstrate the nature of the critical point I, we consider as the order parameter $\Delta M\equiv M-\overline{M}$, where $\overline{M}\equiv(\langle M_a\rangle+\langle M_b\rangle)/2$ and $M_{a,b}$ are the values of M immediately above (below) the first-order line. $M_{a,b}$ are calculated by varying T at fixed $u_{a,b}$, just above (below) $u_0(h=0.3)$. We find that $\overline{M}=0.5$ (within 0.1% error)

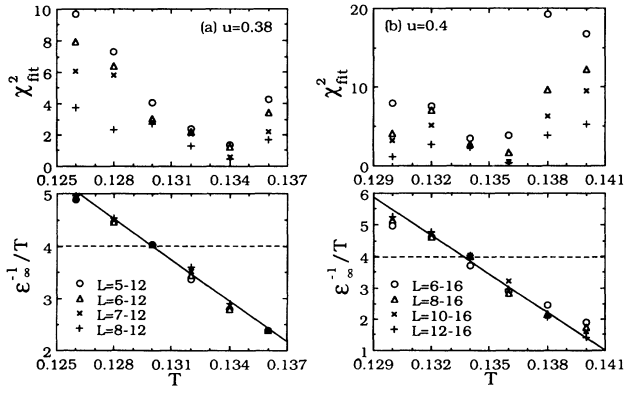

FIG. 8. (a) The χ^2_{fit} error for a fit to Eq. (32) as a function of T, and corresponding fitted value of ϵ_∞^{-1}/T for different sequences of L, for (a) $u=0.5$ and (b) $u=0.63$. In (a), $L=5,6,7,8,10,12$, and (b) $L=6,8,10,12,14,16$, have been used.

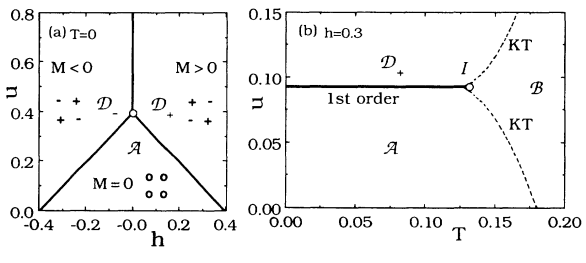

FIG. 9. Phase diagram for the square lattice in an ordering field h. (a) shows the u-h plane at $T=0$. (b) shows the u-T plane at $h=0.3$. The thick solid line is a first-order transition which ends at an Ising critical point I. The dashed lines are Kosterlitz-Thouless transitions which meet the first-order line below I.

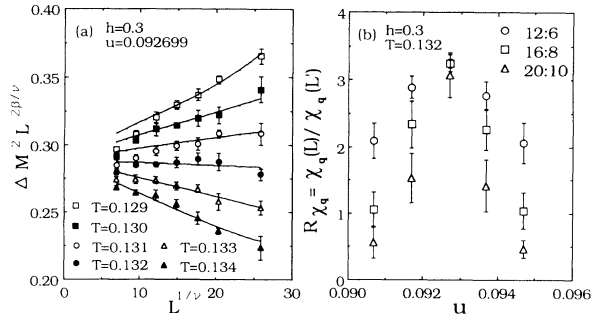

FIG. 10. (a) The finite-size-scaling behavior of the order parameter $(\Delta M)^2$ at $u_0(h=0.3)$. Symbols with error bars represent the MC data. The solid lines represent a result of fitting to Eq. (29) using a fourth-order expansion in $T-T_c$ and data from $L=10$–20. The fitted values of $1/\nu=1.0860$ and $\beta/\nu=0.1458$ were used in making the axes of the plot. (b) Ratio of charge density susceptibility R_{χ_q} vs u, passing through point I [see Fig. 9(b)]. Three different sets of lattice lengths $L:L'$ with the same ratio 2 are shown. The common intersection of the three curves is at $[u_0(h),2^{\gamma/\nu}]$. 10^6 total MC passes were used.

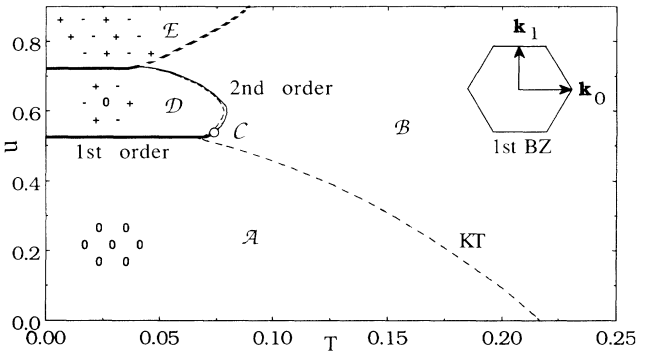

FIG. 11. Phase diagram for the classical neutral integer charge 2D Coulomb gs on a triangular lattice as a function of temperature T and u. As u increases, the average charge density increases. The dashed lines are where the dielectric function ϵ diverges. The thick solid lines are first-order transitions, while the thin solid line is a second-order transition. The dashed lines meet the first-order line below point $\mathcal{C}$. The thick dashed line denotes a crossover region as opposed to a true thermodynamic transition. The insets to $\mathcal{A}$, $\mathcal{D}$, and $\mathcal{E}$ show the ground-state charge configurations in each region.

for all values of T. In Fig. 10(a), we show our data for $(\Delta M)^2$ vs L for different temperatures T. Using the expansion of the order-parameter scaling function Eq. (29), we find from a fit to a fourth-order expansion for our data from sizes $L=10$–20, the critical exponents $\beta/\nu=0.1458\pm0.0269$, $1/\nu=1.0860\pm0.0401$, and $T_c=0.1318\pm0.0008$. These values are consistent with the exact exponents for an Ising transition, $\beta/\nu=0.125$, $1/\nu=1$.

As an independent check, we have also computed the charge susceptibility $\chi_q(u,L)=-T\partial^2 f/\partial u^2$, varying u for fixed $T=T_c$ (with $T_c=0.132$ obtained from the fit to ΔM above). χ_q should scale with the same exponent as the order-parameter susceptibility, $\chi_q \sim L^{\gamma/\nu}$. Plotting the ratio $R_{\chi_q}\equiv\chi_q(L)/\chi_q(L')$ in Fig. 10(b), we find

$$R_{\chi_q}[u_0(h)]=2^{\gamma/\nu}=3.07\pm0.33$$

giving $\gamma/\nu=1.62\pm0.16$. This is consistent with the Ising value $\gamma/\nu=1.75$.

The "metal-insulator" transitions in Fig. 9(b), we analyze as in Section III D, and find that they are consistent with KT universality. These KT transition lines meet the first-order line at a temperature lower than the Ising critical point. This is checked by the similar analysis to that of Sec. III D concerning Fig. 6.

IV. THE INTEGER COULOMB GAS ON A TRIANGULAR LATTICE

A. Phase diagram

For the case of a triangular lattice, our results are summarized by the u-T phase diagram shown in Fig. 11. The small-u (low-density) insulating phase $\mathcal{A}$ is similar to that on the square lattice. The vacuum is the ground state, and increasing T gives a KT "metal-insulator" transition (dashed line) to a conducting phase $\mathcal{B}$.

Increasing u at small T, there is a first-order transition (thick solid line) to an insulating charge lattice phase $\mathcal{D}$. At $T=0$, the ground-state configuration, shown as the inset to phase $\mathcal{D}$ in Fig. 11, has an average $\langle q_i^2\rangle=\frac{2}{3}$, and is six-fold degenerate corresponding to the permutation of the $(+,-,0)$ charges on the three independent sublattice (A,B,C) of the original triangular lattice. At finite T, phase $\mathcal{D}$ is described by a nonvanishing Fourier component of the average charge density $\langle q_{k_0}\rangle$, where $\mathbf{k}_0=(4\pi/3)\hat{\mathbf{a}}_1$ is the ordering wave vector which points to a vertex of the surface of the first Brillouin zone (BZ) (see inset to Fig. 11). All other $\{\mathbf{k}'\}$ which point to the other vertices of the BZ are related to $\mathbf{k}_0$ by inversion symmetry, or translation by a reciprocal-lattice vector. Hence, the other nonvanishing Fourier components, $\langle q_{k'}\rangle$, are all equal either to $\langle q_{k_0}\rangle$, or to $\langle q_{k_0}\rangle^*$. Thus, we take $\psi\equiv\langle q_{k_0}\rangle/N$ as a complex order parameter for phase $\mathcal{D}$. If the state with $(+,-,0)$ on sublattices (A,B,C), has order parameter of value ψ_0, then the six degenerate ground states of the system may be denoted

$$\begin{aligned}&(+,-,0),\\&(0,-,+),\\&(-,0,+),\\&(-,+,0)\\&(0,+,-),\\&(+,0,-)\end{aligned}\qquad(43)$$

with respective order parameters

$$\psi_m=\psi_0 e^{im\pi/3},\quad m=0,\ldots,5 \qquad(44)$$

obtained by successive rotations of the phase of the complex number ψ_0 by $\pi/3$. Equivalently, if ψ is the value of

the order parameter, then $\psi e^{\pm i\pi/3}$ are the values for the state in which either + or − has been interchanged with 0, and ψ^* is the value for the state obtained by charge inversion, $+\leftrightarrow-$.

Increasing T from within $\mathcal{D}$, there is first a "metal-insulating" transition (dashed line) to a conducting phase, followed very closely by a second-order charge lattice melting transition (thin solid line) to phase $\mathcal{B}$. Further increasing u at small T, there is another first-order transition (thick solid line) to a metastable region $\mathcal{E}$, where the ground state at $T=0$ has $\langle q_i^2\rangle=1$, with charges ordered and alternating in one basis direction, but completely random in the other directions. We will show that this state is, in principle, disordered at any finite temperature. As T increases, there is a continuous crossover (thick dashed line) to phase $\mathcal{B}$.

Point $\mathcal{C}$, where the second-order (thin solid) line meets the first-order (thick solid) line between phases $\mathcal{A}$ and $\mathcal{D}$, has behavior suggestive of a multicritical point. The "metal-insulator" (thin dashed) lines meet this first-order line below point $\mathcal{C}$. The point where the second-order line meets the first-order line between $\mathcal{D}$ and $\mathcal{E}$ shows very strong fluctuations and the situation remains unclear.

B. First-order transitions

As in the square lattice (see Sec. III B), the locations of the first-order transition lines are given by considering the Fourier transform of the Hamiltonian, Eq. (33). For the triangular lattice, with V_k given by Eq. (6), $\min_k[V_k]=\pi/3$ occurs at $\mathbf{k}_0$, the ordering wave vector of phase $\mathcal{D}$. Therefore, when $u>u_0=\pi/6=0.523\,60$, the system will prefer to order in a state with nonvanishing $\langle q_{k_0}\rangle$. This is the charge structure, shown in phase $\mathcal{D}$ of Fig. 11, with $\langle q_i^2\rangle=|q_{k_0}|^2/N^2=\frac{2}{3}$, and energy

$$E=(\pi/6-u)(2/3)N\ . \tag{45}$$

As u increases further, the system will eventually prefer a ground state with higher charge density, $\langle q_i^2\rangle=1$. The most symmetric state with this density would have alternating ±1 charges along one of the directions $\hat{\mathbf{a}}_i$, and be uniform along the other basis direction. Such a state would have periodicity given by a wave vector pointing to the center of one of the faces of the first BZ, for example, $\mathbf{k}_1=(2\pi/\sqrt{3})\hat{\mathbf{y}}$ (see inset in Fig. 11), with $V_{k_1}=3\pi/8$. However, from Eq. (6), it is seen that for *any* $\mathbf{k}$ such that $\mathbf{k}\cdot\hat{\mathbf{a}}_i=\pm\pi$, $V_k=V_{k_1}$. Thus, all of the 2^L states with alternating charges along a given $\hat{\mathbf{a}}_i$, but arbitrary ordering in the second basis direction, are degenerate with energy

$$E=(3\pi/16-u)(1)N\ . \tag{46}$$

Comparing Eqs. (45) and (46), we see that such a configuration, which we denote as $\mathcal{E}$, becomes the ground state, with lower energy than the configuration $\mathcal{D}$, when $u>u_1=11\pi/48=0.719\,95$.

The points u_0 and u_1, where there are discontinuous changes in the ground state, extend into the first-order lines of Fig. 11 at finite T. We have numerically evaluated the surface tension between regions $\mathcal{D}$ and $\mathcal{E}$ at $T=0$, and find that $\sigma_{\mathcal{D},\mathcal{E}}\simeq0.05$. This is equal to the approximate temperature at which we numerically observe the first-order line between $\mathcal{D}$ and $\mathcal{E}$ to meet the second-order line between $\mathcal{D}$ and $\mathcal{B}$.

C. Charge lattice melting transition

We now consider the second-order transition between phases $\mathcal{D}$ and $\mathcal{B}$. As discussed in Sec. IV A, the complex order parameter describing the charge lattice configuration (see inset phase $\mathcal{D}$, Fig. 11) is $\psi=\langle q_{k_0}\rangle/N$, which below T_c can take the six values $\psi_m=\psi_0(T)e^{im\pi/3}$, $m=0,\ldots,5$. Viewing ψ as a two-component planar spin suggests a mapping between this phase and behavior in the six-state clock model.

In the six-state clock model, each site of the lattice contains a planar spin which can point in only one of six directions, with angles $\theta_m=m\pi/3$, $m=0,\ldots,5$. The interaction between neighboring spins, with angle difference $\Delta\theta$, is $V(|\Delta\theta|)$. If we normalize V so that $V(0)\equiv0$, the most general six-state clock model is characterized by three parameters, $V(\pi/3)$, $V(2\pi/3)$, and $V(\pi)$. For the special cases[33] $V(|\Delta\theta|)=V_0[1-\cos(\Delta\theta)]$ or $V(|\Delta\theta|)$, the Villain function[34] (we refer to these two cases as the *usual* six-state clock model), this model in two dimensions is known to have an intermediate phase with algebraic decay in the spin-spin correlation. This intermediate phase is terminated at both the low- and high-temperature ends by a Kosterlitz-Thouless-like transition. For other choices of $V(|\Delta\theta|)$, a single first-order transition may be possible, as suggested by the mean-field analysis of Domany and Riedel,[35] or the example of $V(|\Delta\theta|)=V_0$, which is the six-state Potts model.[36]

For our phase $\mathcal{D}$, we estimate the form for the effective $V(|\Delta\theta|)$ by numerically calculating the surface tension between the six ground states of the system at $T=0$. If θ is the phase of the order parameter ψ, then the surface tensions we find between the six ground states as denoted in Eqs. (43) and (44) give an excellent fit to the expression $\sigma(|\Delta\theta|)=0.103[1-\cos(\Delta\theta)]$. The prefactor gives a rough estimate of the temperature of the second-order melting line in Fig. 11. Provided that this cosine interaction, which we find at $T=0$, remains qualitatively unchanged at finite T, we would expect the melting transition of phase $\mathcal{D}$ to have the intermediate algebraic phase of the usual six-state clock model. This expectation is further supported by a Landau-like symmetry analysis. Under such analysis, Domany *et al.*[37] have classified possible order-disorder transitions in two-dimensional adsorbed monolayers on a substrate. The symmetry of the charge lattice lattice in phase $\mathcal{D}$, in their classification scheme, is denoted as $(\sqrt{3}\times\sqrt{3})R30$ with particle-hole symmetry [corresponding to the invariance of our Hamiltonian (10) under $q_i\leftrightarrow-q_i$]. Such a system is predicted to be in the universality class of the XY model with sixfold anisotropy,[3] which is the same universality class as the usual six-state clock model.

According to the above scenario, we would expect to

see only a finite cusp in the specific heat C (or perhaps two cusps, if one could distinguish the transitions on either end of the expected intermediate phase) due to the KT-like nature of the transitions. In our case, however, we observe a diverging specific heat C at a single transition. To determine the scaling exponent for C, we use the ratio method of Sec. II C. In Fig. 12(a), we plot $R_c = C(L)/C(L')$ vs T for ratios $L/L' = \frac{12}{6}, \frac{18}{9}$, and $\frac{24}{12}$ at $u = 0.63$. The three curves intersect at a single point with $T_c = 0.078$, $R_C = 2^{\alpha/\nu} = 2.0 \pm 0.2$, thus giving $\alpha/\nu = 1.00 \pm 0.14$. Hyperscaling, $\alpha = 2 - d\nu$ then gives $1/\nu = 1.5 \pm 0.07$. Similar calculations at $u = 0.60$ and 0.66 give values $\alpha/\nu = 0.97 \pm 0.14$ and 1.10 ± 0.24.

To determine the critical exponent for the order parameter, we compute $|\psi|^2$ vs T for fixed $u = 0.63$. In Fig. 12(b), we show our results for lattice sizes $L = 6$–24. Fitting to the scaling form Eq. (29), and using data from sizes $L = 9$–24 with a fourth-order expansion, we find $\beta/\nu = 0.04 \pm 0.01$, $1/\nu = 1.47 \pm 0.05$, and $T_c = 0.0773 \pm 0.0003$. These results agree with the above scaling results for C. The solid lines in Fig. 12(b) are plotted from Eq. (29) using the fitted values of the parameters.

We thus have evidence suggesting that the melting transition of phase $\mathcal{D}$ does not follow the expectations of a Landau symmetry analysis. We have explicitly checked for the possibility that the transition we see might be first order by looking for hysteresis as well as looking for a bimodal energy distribution near T_c (in which case one should find scaling as $C \sim L^d$). We did not find any evidence for either such signature of a first-order transition. We, of course, cannot rule out a sufficiently weak first-order transition which would be observable only at larger lattice sizes.

In contrast to the above results along the second-order line, our results at the point $u = 0.54$, where the second-order line meets the first-order line at $\mathcal{C}$ show different scaling behavior. A similar ratio analysis[18(b)] at point $\mathcal{C}$ gives the exponent $\alpha/\nu = 1.51 \pm 0.15$ or $1/\nu = 1.755 \pm 0.07$. One possible explanation is that $\mathcal{C}$ is a multicritical point.

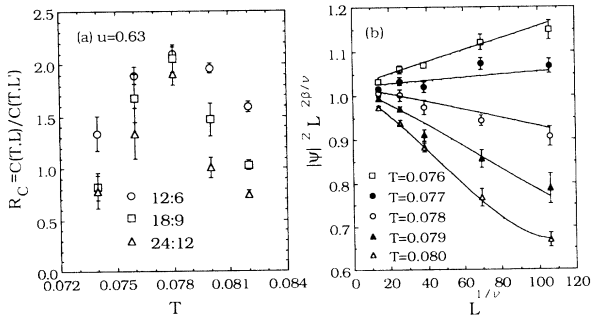

FIG. 12. (a) Ratio of specific heats R_C vs T at $u = 0.63$ in phase $\mathcal{D}$. Three different sets of lattice lengths $L:L'$ with equal ratio 2 are shown. The common interaction of the three curves is at $(T_c, 2^{\alpha/\nu})$. (b) The finite-size-scaling behavior of the order parameter $|\psi|^2$ at $u = 0.63$. Symbols with error bars represent the MC data. The solid lines represent the results of fitting Eq. (29) to a fourth-order expansion in $T - T_c$ using data from $L = 9$–24. The fitted values of $1/\nu = 1.47$ and $\beta/\nu = 0.04$ were used in making the axes of the plot. 10^6 total MC passes were used.

D. Metal-insulator transition

Next we consider the "metal-insulator" transitions (dashed lines in Fig. 11). As in Sec. III D, we find that as one crosses from phase $\mathcal{A}$ to $\mathcal{B}$, the peak of the specific heat C ultimately saturates to a finite value as L increases, consistent with a KT transition. The "metal-insulator" phase boundaries (dashed lines in Fig. 11) are determined in the same way as on the square lattice (see Figs. 5 and 6), and we again find that these lines meet the first-order line between phases $\mathcal{A}$ and $\mathcal{D}$, *below* point $\mathcal{C}$.

In Figs. 13(a) and 13(b), we show the finite-size-scaling behavior of $\epsilon^{-1}(T,L)$ for $u = 0.5$ (in phase $\mathcal{A}$ just below the first-order line) and $u = 0.63$ (in phase $\mathcal{D}$), respectively. Comparing the estimate for T_c given by the point at which the curves for different L intersect [see discussion by Eq. (31)], with the KT bound Eq. (30) given by the intersection with the dashed line $4T$, we see that, for $u = 0.5$, $\epsilon^{-1}(T_c) \simeq 4T_c$, consistent with the KT universal jump of the ordinary dilute ($u = 0$) CG. However, at $u = 0.63$, we find that the estimate of T_c gives a jump larger than the universal KT value, $\epsilon^{-1}(T_c) > 4T_c$. Similar nonuniversal jumps are found at other u in $\mathcal{D}$.

As a more precise test, we carry out finite-size-scaling fits to Eq. (32), as was done for the square lattice in Sec. III D. In Fig. 14, we show vs T the $\chi^2_{\rm fit}$, together with the fitted parameter ϵ_∞^{-1}, for the two values of u in Fig. 13. For $u = 0.5$, we see that the minimum of $\chi^2_{\rm fit}$ occurs where $\epsilon_\infty^{-1} = 4T$, consistent with the KT universal jump. For $u = 0.63$, we see that, at the T where $\chi^2_{\rm fit}$ is minimum, $\epsilon_\infty^{-1} > 4T$, consistent with a larger than universal jump. These results thus support the conclusions of Fig. 13. The transition temperature of this "metal-insulator" transition at $u = 0.63$, as given by the minimum $\chi^2_{\rm fit}$ in Fig. 14(b), is $T_c = 0.076$. In contrast, the melting transition temperature of the charge lattice of phase $\mathcal{D}$, as obtained from the analysis of specific heat C in Fig. 12(a), is $T_c = 0.078$. This suggests that, as T is increased within phase $\mathcal{D}$, there is first a "metal-insulating" transition to an intermediate conducting phase with finite charge lattice order, followed very closely by the charge lattice melting transition.

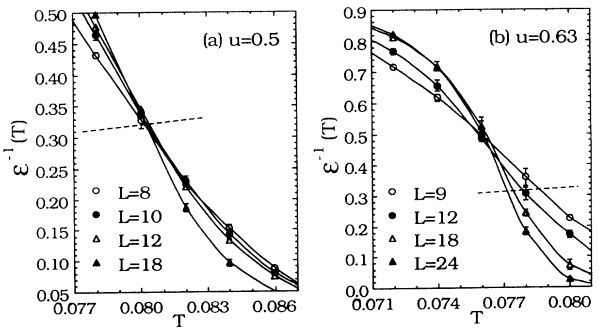

FIG. 13. Inverse dielectric function $\epsilon^{-1}(T,L)$ vs T for (a) $u = 0.5$ (just below the first-order line) in $\mathcal{A}$, and (b) $u = 0.63$ in $\mathcal{D}$ for various triangular lattice sizes L. The common intersection of the curves for different L gives an estimate for T_c. Intersection with the dashed line $4T$ gives the Kosterlitz-Thouless upper bound on T_c. 10^6 total MC passes were used.

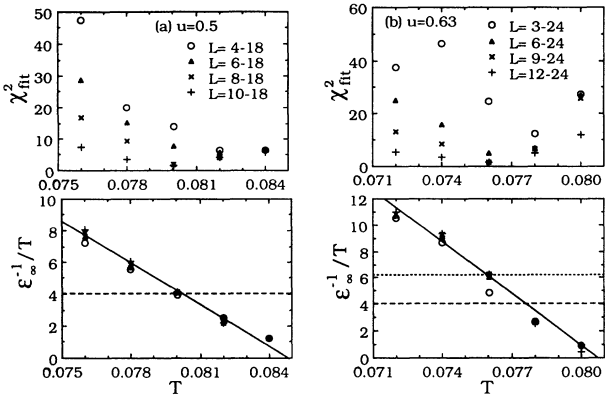

FIG. 14. The $\chi^2_{\rm fit}$ error for a fit to Eq. (32) as a function of T and corresponding fitted value of ϵ_∞^{-1}/T for different sequences of L for (a) $u=0.5$ and (b) $u=0.63$. In (a) $L=4,6,8,10,12,18$, and (b) $L=3,6,9,12,18,24$, have been used.

E. Metastable region at large densities

Finally, we consider the metastable region, denoted as $\mathcal{E}$ in Fig. 11. In this region at low T, every site contains either a $+1$ or -1 charge. Thus, it has the symmetry of the Ising antiferromagnet. In the short-range Ising antiferromagnet on a triangular lattice,[38] frustration results in an infinitely degenerate ground state, with a finite $T=0$ entropy density, and $T_c=0$. However, in the CG, the long-range interactions lift some of the degeneracies caused by the frustration, giving an antiferromagnetic order in one of the directions $\hat{\mathbf{a}}_i$. The remaining randomness in the other direction leads to a ground-state degeneracy of 2^L, which gives a vanishing $T=0$ entropy density, $\ln(2^L)/L^2\to 0$ as $L\to\infty$. One might thus expect that a finite T_c is possible. In Figs. 15(a)–15(c), we show for $u=0.8$ the specific heat C, inverse dielectric constant ϵ^{-1}, and average charge density $\langle q_i^2\rangle$. The sharp transitions seen in C and ϵ^{-1} suggest a possible transition at finite T_c. Furthermore, hysteresis loops for $\langle q_i^2\rangle$ might indicate that the transition from $\mathcal{E}$ to $\mathcal{B}$ is first order. However, we now argue that this behavior is, in fact, merely a nonsingular crossover region to the disordered phase $\mathcal{B}$.

In Fig. 15(d), we show two types of domain excitations of a ground state. Each is formed by taking a strip of even length l of the ground state and reversing the sign of all the charges in the strip. In type (ii), the strip is chosen so that the net dipole moment of the excitation, with respect to the ground state, vanishes. In type (i), the charges at the ends of the strip are replaced by vacancies, to again give a vanishing net dipole moment. In Fig. 16, we plot the numerically computed excitation energies $\Delta E(l)$ of these domains, using only the Coulomb interaction part of the Hamiltonian, Eq. (9). For type (i), we see that ΔE approaches a finite constant $\simeq 0.79$ for $l\gtrsim 10$. Including the chemical potential term in u, Eq. (10), we have $\Delta E(u)\simeq 0.79+2u$, where the second term comes from the two vacancies. For domains of type (ii), $\Delta E\simeq 4.9$ for $l\gtrsim 10$, independent of u. In each case, we find the excitation energy is essentially independent of which ground state is chosen as the background. Since ΔE approaches a finite constant in both caes, once a large enough ($l\gtrsim 10$) domain is created, there is no further cost in energy to increase the domain length, and as a result the domain may grow and the system may switch to a different ground state. Since there is always a finite probability $\sim e^{-\Delta E/T}$ to create such domains at any $T>0$, the ground state order will be destroyed at any finite T. This is analogous to the case of the 1D Ising model, in which domain-wall excitations destroy the ground-state order at any $T>0$ and lead to $T_c=0$. Thus, the apparent transition seen in Fig. 15 is just a crossover region where these domain excitations proliferate, and the true transition temeprature is at $T=0$.

From Fig. 15(b), it appears that these domain excitations also drive $\epsilon^{-1}\to 0$. In Fig. 17 (a), we plot ϵ^{-1} for various lattice sizes L, using the same number of MC steps. In Fig. 17(b), we plot ϵ^{-1} for fixed L but different numbers of MC steps. We see that an increase in either the lattice size or in the number of MC steps causes a downward shift in the apparent transition temperture where $\epsilon^{-1}\to 0$. As we expect that there is a constant rate per unit area per unit time to create the critical domain excitations of Fig. 15(d), increasing either L or the num-

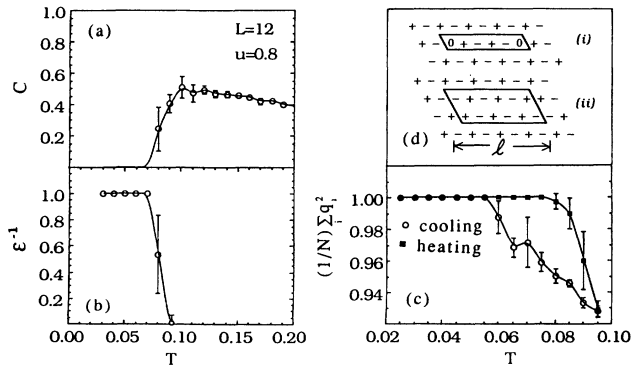

FIG. 15. (a) Specific heat C, (b) inverse dielectric function ϵ^{-1}, and (c) average charge density $\langle q_i^2\rangle$ vs T at $u=0.8$ in region $\mathcal{E}$. (d) shows two types of domain excitations that disorder the ground state. In (a)–(c), 60 000 total MC passes on an $L=12$ triangular lattice were used.

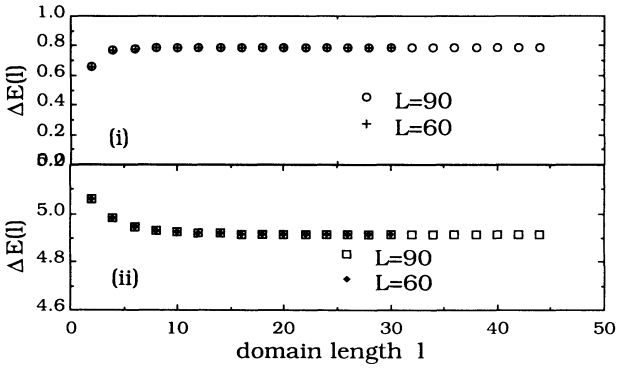

FIG. 16. Domain excitation energies $\Delta E(l)$ as a function of domain length l for the two types of domains considered in Fig. 15(d). As $l\to\infty$, ΔE remains finite in each case.

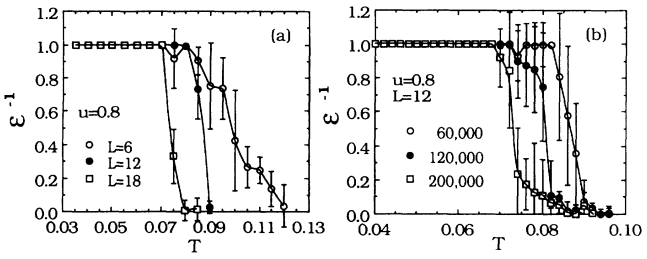

FIG. 17. Inverse dielectric function ϵ^{-1} vs T at $u=0.8$ in region $\mathcal{E}$ for (a) a fixed number of 60 000 total Monte Carlo steps but different lattice sizes L, and for (b) a fixed lattice size $L=12$ but different number of total Monte Carlo steps.

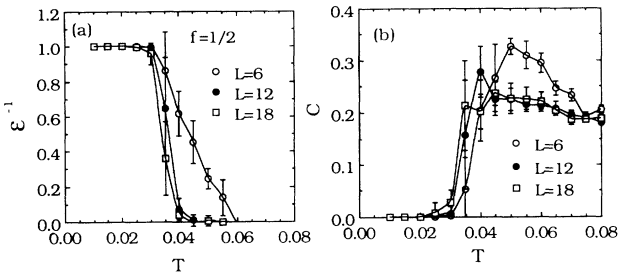

FIG. 18. (a) Inverse dielectric function $\epsilon^{-1}(T)$ and (b) specific heat $C(T)$ for various triangular lattice sizes, L, for $f=\frac{1}{2}$. 60 000 total MC passes were used.

ber of MC steps are equivalent ways to increase the number of such excitations created in a given simulation. We therefore expect that, in the limit $L\to\infty$ for infinitely long simulation times, we would find $\epsilon^{-1}\to 0$ at any finite T.

V. THE FRACTIONAL COULOMB GAS ON A TRIANGULAR LATTICE

We now consider the case of the fractional Coulomb gas on the triangular lattice given by the Hamiltonian (9) with fractional charges as in Eq. (11), $q_i=n_i-f$, n_i integer. The charges in this model may be mapped onto the vortices in the uniformly frustrated XY model on the dual honeycomb lattice,[3,8,9] which serves as a model for a Josephson-junction array (JJA) in a transverse magnetic field. In this mapping, f is the number of flux quantum of applied magnetic field per unit cell of the array. We consider the two cases $f=\frac{1}{2}$ and $\frac{1}{3}$.

A. $f=\frac{1}{2}$

The $f=\frac{1}{2}$ case has been previously investigated in the context of the "fully frustrated" JJA on a honeycomb lattice. Monte Carlo simulations of the corresponding XY model have been carried out,[39] and the degeneracy of the ground state has been discussed.[40] In the Coulomb gas formulation, the system consists at low temperatures of equal numbers of $\pm\frac{1}{2}$ charges, and the ground states correspond to those of region $\mathcal{E}$ in the dense integer CG, discussed in Sec. IV E. The primary difference from region $\mathcal{E}$ is that vacancies are no longer a permitted excitation. It is therefore expected that domain excitations of type (ii), as shown in Fig. 15(d), will destroy the ground-state order in this system at any finite $T>0$.

We have carried out independent simulations of the $f=\frac{1}{2}$ CG and present our results for ϵ^{-1} and C vs T in Figs. 18(a) and 18(b). The results show very similar behavior to that seen in Figs. 15(a) and 15(b) for region $\mathcal{E}$ of the dense integer charge model. They are also qualitatively similar to the results of Shih and Stroud[39] for the helicity modulus Υ and C in the corresponding XY model once one considers that the smooth background spin-wave excitations present in the XY model have been discarded in the mapping[3] to the CG. As in Fig. 17 for region $\mathcal{E}$ of the integer model, we see that ϵ^{-1} shows a downward shift in the apparent transition temperature, as the size of system is increased. Therefore, we believe that the $f=\frac{1}{2}$ model, similar to region $\mathcal{E}$, has $T_c=0$.

B. $f=\frac{1}{3}$

In the $f=\frac{1}{3}$ model at low temperatures, the system consists of a $\frac{1}{3}$ density of charges $q=+\frac{2}{3}$ and a $\frac{2}{3}$ density of charges $q=-\frac{1}{3}$. There are three degenerate ground states, which we may denote by $(+,-,-)$, $(-,+,-)$, and $(-,-,+)$, according to which charges sit on the three independent sublattices (A,B,C) of the triangular lattice. The ground state has the same periodicity as phase $\mathcal{D}$ of the integer charge model, discussed in Secs. IV A and IV C. It is characterized by the complex order parameter $\psi=\langle q_{k_0}\rangle/N$, with the same wave vector $\mathbf{k}_0$ as in Fig. 11. The three-fold degeneracy corresponds to rotations of the phase of the complex order parameter ψ by $2\pi/3$. A symmetry analysis[37] predicts the melting transition of this charge lattice to be in the universality class of the three-state Potts model.

In Fig. 19(a) we use the ratio method and plot $R_C=C(L)/C(L')$ for ratios $L/L'=\frac{12}{6}$, $\frac{18}{9}$, and $\frac{24}{12}$. From the common intersection of the three curves, we get $T_c=0.76$ and $R_C(T_c)=2^{\alpha/\nu}=2.22\pm0.21$, giving $\alpha/\nu=1.15\pm0.11$ and $1/\nu=1.58\pm0.06$. These values are approximately the same as found in the melting transition of phase $\mathcal{D}$ in the integer charge model.

In Fig. 19(b), we plot the square of the order parameter $|\psi|^2$ for $L=6$–24. From a fit to the fourth-order expansion of the scaling equation, Eq. (29), using data from $L=12$–24, we find $\beta/\nu=0.09\pm0.03$, $1/\nu=1.59\pm0.07$, and $T_c=0.0755\pm0.0002$, consistent with the analysis of C. In contrast, the exact exponents[41] for the two-dimensional three-state Potts model are $\beta/\nu=\frac{2}{15}=0.1333$, $1/\nu=\frac{6}{5}=1.2$, and $\alpha/\nu=\frac{2}{5}=0.4$.

In Fig. 20, we plot $\epsilon^{-1}(T,L)$ vs T for various sizes L. The intersection of the curves with the dashed line $4T$ gives the KT upper bound on T_c, which is noticeably higher than the estimate of T_c given by the common intersection of the curves for different L. This suggests that $\epsilon^{-1}(T_c)$ has a possibly larger jump to zero at T_c than the universal KT value. Comparison of Figs. 19(a) and 20 suggests that ϵ^{-1} vanishes at a temperature slightly lower than the melting temperature where the order parameter ψ vanishes.

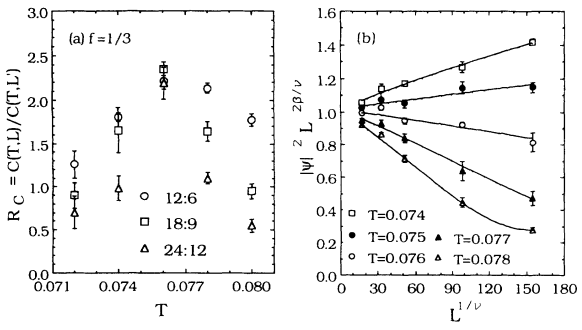

FIG. 19. (a) Ratios of specific heats R_C vs T for $f=\frac{1}{3}$. Three different sets of lattice lengths $L:L'$ with equal ratio 2 are shown. The common intersection of the three curves is at $(T_c, 2^{\alpha/\nu})$. (b) The finite-size-scaling behavior of the order parameter $|\psi|^2$ for $f=\frac{1}{3}$. Symbols with error bars represent the MC data. The solid lines represent the result of fitting Eq. (29) to a fourth-order expansion in $T-T_c$ using data from $L=12$–24. The fitted values of $1/\nu=1.59$ and $\beta/\nu=0.09$ were used in making the axes of the plot. 10^6 total MC passes were used.

VI. CONCLUSION

We have carried out extensive Monte Carlo simulations of the integer and fractional two-dimensional Coulomb gases, on square and triangular lattices, and have found rich critical behavior. One of our goals has been to investigate whether the discontinuous jump to zero of the inverse dielectric constant ϵ^{-1} at the "metal-insulator" transition might be larger than the universal Kosterlitz-Thouless value $\epsilon^{-1}(T_c)=4T_c$ once the charge density is sufficiently large. Such a possibility has been suggested by Minnhagen[11,12] for the dense Coulomb gas in a continuum. We find that whenever the ground state of the system is the charge vacuum (phase $\mathcal{A}$), there is no strong evidence for anything but the universal KT behavior, no matter how dense the system. When the ground state is a charge lattice, however, we find some evidence for a possibly larger than universal jump for phase $\mathcal{D}$ of the integer model and for the $f=\frac{1}{3}$ fractional model, both on the triangular lattice. This may be due to the coupling of domain excitations of the charge lattice with the pair unbinding excitations of the Kosterlitz-Thouless theory. Although our phase diagrams do not agree quantitatively with those predicted by Minnhagen, some qualitative similarities do exist. In both cases, the "dilute" phase (our phase $\mathcal{A}$) is bounded by a line of KT transitions which meet a first-order line at a temperature *below* the end point of the first-order line. Across the first-order line there is a discontinuous jump in charge density. In Minnhagen's calculations, the dense phase above the first-order line is a dense charge fluid, where $\epsilon^{-1}=0$. The nonuniveral jump in ϵ^{-1} in his model comes from crossing this first-order line. Some evidence for this picture has been found in Monte Carlo simulations for the continuum integer Coulomb gas on the surface of a sphere by Caillol and Levesque.[42] In our model, the dense phase above the first-order line is an ordered charge lattice with $\epsilon^{-1}>0$. The ordering into a charge lattice is a direct consequence of having our charges sit on discrete periodic sites rather than being in a continuum. We therefore cannot rule out the behavior suggested by Minnhagen for the continuum model.

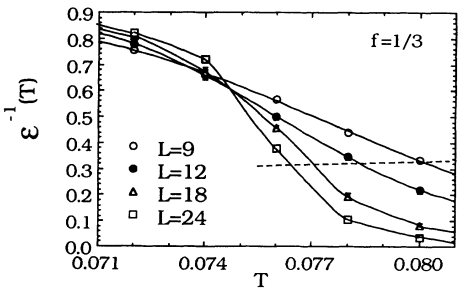

FIG. 20. Inverse dielectric function $\epsilon^{-1}(T,L)$ vs T for $f=\frac{1}{3}$ for various triangular lattice sizes L. The common intersection of the curves for different L gives an estimate for T_c. Intersection with the dashed line $4T$ gives the Kosterlitz-Thouless upper bound on T_c. 10^6 total MC passes were used.

A second goal of our investigations has been to determine whether the melting transitions of Coulomb interacting charge lattices can be classified by the type of symmetry analysis used for short-range-interaction models. Here we have found several examples where the critical behavior we find does not agree with that expected from symmetry. For the tricritical point of the integer model on the square lattice, we find $\alpha/\nu\simeq 1.1$, compared to the Ising tricritical $\alpha/\nu=1.6$. For the melting of the six-fold degenerate phase $\mathcal{D}$ of the triangular lattice, we find $\alpha/\nu\simeq 1.0$, different from the expected KT behavior of the six-state clock model. For the melting of the three-fold degenerate phase of the $f=\frac{1}{3}$ fractional model on the triangular lattice, we find $\alpha/\nu\simeq 1.15$, as compared to the expected value for the three-state Potts model $\alpha/\nu=0.4$. At the apparent multicritical point $\mathcal{C}$ of the integer model on the triangular lattice, we find $\alpha/\nu\simeq 1.5$. The exponents we find have consistent values when obtained from different finite-size-scaling methods, applied to different physical quantities. We have no clear explanation for the failure to agree with symmetry predictions, nor why, in the first three of our above examples, we find the same value $\alpha/\nu\simeq 1$. One possibility might lie in the very long-range nature of the Coulomb interactions. We, of course, cannot rule out the possibility that all these transitions are really weakly first order, which would only become evident when studying larger lattice sizes (where we would expect to see an apparent $\alpha/\nu=d=2$ coming from the bimodal energy distribution at a first-order transition).

ACKNOWLEDGMENTS

It is a pleasure to thank Professor P. Minnhagen, Professor E. Domany, Professor K. K. Mon, Professor Y. Shapir, and Dr. Y.-H. Li for valuable discussions in the course of this work. This work was supported by the U.S. Department of Energy under Grant No. DE-FG02-89ER14017.

[1]For a review, see (a) P. Minnhagen, Rev. Mod. Phys. **59**, 1001 (1987); (b) B. Nienhuis, in *Phase Transitions and Critical Phenomena,* edited by C. Domb and J. Lebowitz (Academic, London, 1987), Vol. 11, p. 1.

[2]J. M. Kosterlitz and D. Thouless, J. Phys. C **6**, 1181 (1973); J. M. Kosterlitz, *ibid.* **7**, 1046 (1974); A. P. Young, *ibid.* **11**, L453, (1978).

[3]J. V. José, L. P. Kadanoff, S. Kirkpatrick, and D. R. Nelson, Phys. Rev. B **16**, 1217 (1977).

[4]B. I. Halperin and D. R. Nelson, J. Low Temp. Phys. **36**, 599 (1979).

[5]D. R. Nelson and J. M. Kosterlitz, Phys. Rev. Lett. **39**, 1201 (1977).

[6]P. Minnhagen and G. G. Warren, Phys. Rev. B **24**, 2526 (1981).

[7]T. Ohta and D. Jasnow, Phys. Rev. B **20**, 130 (1979).

[8]S. Teitel and C. Jayaprakash, Phys. Rev. B **27**, 598 (1983).

[9]S. Teitel and C. Jayaprakash, Phys. Rev. Lett. **51**, 1999 (1983).

[10]B. I. Halperin, in *Physics of Low-Dimensional Systems,* Proceedings of the Kyoto Summer Institute, edited by Y. Nagaoka and S. Hikami (Publication Office, Prog. Theor. Phys., Kyoto, 1979), p. 53; D. R. Nelson, in *Phase Transitions and Critical Phenomena,* edited by C. Domb and J. Lebowitz (Academic, London, 1983), Vol. 7, p. 1; K. J. Strandburg, Rev. Mod. Phys. **60**, 161 (1988).

[11]P. Minnhagen, Phys. Rev. Lett. **54**, 2351 (1985); Phys. Rev. B **32**, 3088 (1985); P. Minnhagen and M. Wallin, *ibid.* **36**, 5620 (1987).

[12]J. M. Thijssen and H. J. F. Knops, Phys. Rev. B **38**, 9080 (1988); P. Minnhagen and M. Wallin, *ibid.* **40**, 5109 (1989).

[13]S. Miyashita and H. Siba, J. Phys. Soc. Jpn. **53**, 1145 (1984); D. H. Lee, J. D. Joannopoulos, J. W. Negele, and D. P. Landau, Phys. Rev. B **33**, 450 (1986); B. Berge, H. Diep, A. Ghazali, and P. Lallemand, *ibid.* **34**, 3177 (1986); J. M. Thijssen and H. J. F. Knops, *ibid.* **37**, 7738 (1988); H. Eikmans, J. E. van Himbergen, H. J. F. Knops, and J. M. Thijssen, *ibid.* **39**, 11 759 (1989).

[14]G. S. Grest, Phys. Rev. B **39**, 9267 (1989).

[15]P. Minnhagen, Phys. Rev. B **32**, 7548 (1985).

[16]J. M. Thijssen and H. J. F. Knops, Phys. Rev. B **42**, 2438 (1990); D. B. Nicolaides, J. Phys. A **24**, L231 (1991).

[17]J. Lee, J. M. Kosterlitz, and E Granato, Phys. Rev. B **43**, 11 531 (1991); E. Granato, J. M. Kosterlitz, J. Lee, and M. P. Nightingale, Phys. Rev. Lett. **66**, 1090 (1991).

[18](a) J.-R. Lee and S. Teitel, Phys. Rev. Lett. **64**, 1483 (1990); (b) **66**, 2100 (1991).

[19]M. N. Barber, in *Phase Transitions and Critical Phenomena,* edited by C. Domb and J. L. Lebowitz (Academic, New York, 1983), Vol. 8, p. 146.

[20]M. P. Nightingale, J. Appl. Phys. **53**, 7927 (1982).

[21]M. N. Barber and W. Selke, J. Phys. A **15**, L617 (1982).

[22]M. P. Nightingale and H. W. Blöte, Phys. Rev. Lett. **60**, 1562 (1988).

[23]S.-K. Ma, *Modern Theory of Critical Phenomena* (Benjamin, Reading, MA, 1976), p. 152.

[24]H. E. Stanley, *Introduction to Phase Transitions and Critical Phenomena* (Oxford University Press, Oxford, 1971).

[25]W. H. Press, B. Flannery, S. A. Teukolsky, and W. T. Vetterling, *Numerical Recipes* (Cambridge University Press, Cambridge, 1986), pp. 521–528.

[26]B. D. Josephson, Phys. Lett. **21**, 608 (1966); M. E. Fisher, M. N. Barber, and D. Jasnow, Phys. Rev. A **8**, 1111 (1973).

[27]H. Weber and P. Minnhagen, Phys. Rev. B **37**, 5986 (1988).

[28]For a review, see I. D. Lawrie and S. Sarbach, in *Phase Transitions and Critical Phenomena,* edited by C. Domb and J. Lebowitz (Academic, London, 1984), Vol. 9, p. 1.

[29]Detailed tables of parameters for this and all similar fits in this paper may be obtained from the authors.

[30]The value of β/ν cited in Ref. 18(a) was incorrectly given as $\frac{1}{2}$ the value cited in the present work.

[31]M. Blum, V. J. Emery, and R. B. Griffiths, Phys. Rev. A **4**, 1071 (1971).

[32]J. Tobochnik and G. V. Chester, Phys. Rev. B **20**, 3761 (1979).

[33]J. Tobochnik, Phys. Rev. B **27**, 6927 (1983); M. S. S. Challa and D. P. Landau, *ibid.* **33**, 437 (1986); A. Yamagata and I. Ono, J. Phys. A **24**, 265 (1991).

[34]S. Elitzur, R. B. Pearson, and J. Sigemitsu, Phys. Rev. D **19**, 3698 (1979).

[35]E. Domany and E. K. Riedel, Phys. Rev. B **19**, 5817 (1979).

[36]R. J. Baxter, J. Phys. C **6**, L455 (1973).

[37]E. Domany, M. Schick, J. S. Walker, and R. B. Griffiths, Phys. Rev. B **18**, 2209 (1978).

[38]R. M. F. Houtappel, Physica (Utrecht) **16**, 425 (1950).

[39]W. Y. Shih and D. Stroud, Phys. Rev. B **30**, 6774 (1984).

[40]S. E. Korschunov, J. Stat. Phys. **43**, 17 (1986).

[41]F. Y. Wu, Rev. Mod. Phys. **54**, 235 (1982).

[42]J. M. Caillol and D. Levesque, Phys. Rev. B **33**, 499 (1986).